PROCEEDINGS OF THE INTERNATIONAL CONFERENCE NANOMATERIALS: APPLICATIONS AND PROPERTIES
Vol. **1** No 3, 03PCSI19(5pp) (2012)

First-Principles Quantum Molecular Dynamics Study of $Ti_xZr_{1-x}N(111)/SiN_y$ Heterosrtructures

V. Ivashchenko[1], S. Veprek[2], A.D. Pogrebnjak[3]

[1] *Institute of Problems of Material Science, NAS of Ukraine, Krzhyzhanovsky str. 3, 03142 Kyiv, Ukraine*
[2] *Department of Chemistry, Technical University Munich, Lichtenbergstrasse 4, D-85747 Garching, Germany*
[3] *Sumy State University, Rymsky-Korsakov str. 2, 40007 Sumy, Ukraine*

(Received 30 May 2012; revised manuscript received 12 July 2012; published online 14 August 2012)

Heterostructures with 1 monolayer of Si_3N_4-like Si_2N_3 interfacial layer between five monolayers thick B1-$Ti_xZr_{1-x}N(111)$, x = 1.0, 0.6, 0.4 and 0.0, slabs were investigated by means of first-principles quantum molecular dynamics and structure optimization procedure using the Quantum ESPRESSO code. Slabs consisting of stoichiometric TiN and ZrN and random, as well as segregated B1-$Ti_xZr_{1-x}N(111)$ solutions were considered. The calculations of the B1-$Ti_xZr_{1-x}N$ solid solutions as well as of the heterostructures showed that the pseudo-binary TiN-ZrN system exhibits a miscibility gap. The segregated heterostructures in which the Zr atoms surround the Si_yN_z interface were found to be most stable. For the Zr-rich heterostructures, the total energy of the random solid solution was lower compared to that of the segregated one, whereas for the Ti-rich heterostructures the opposite tendency was observed.

Keywords: Ti-Zr-N/SiN_x Nanolayered Coatings, Interface, First-Principles Investigation, Quantum Molecular Dynamics.

PACS numbers: 31.15.at, 81.07.Nb

1. INTRODUCTION

The superhard nanocomposites and nanolayered heterostructures exhibit enhanced hardness of 40-100 GPa and ≤ 35 GPa, respectively, combined with high thermal stability [1-5] which is somewhat lower for the heterostructures [6] as compared with the nanocomposites [1]. The large increase of the hardness in the nanocomposites as compared with TiN (20-21 GPa) has been attributed to the 3-4 nm size TiN grains which prevents dislocation activity, and one monolayer interfacial SiN_x [7] which is strengthened by valence charge transfer [8]. The SiN_x tissue connecting the grains enhances the strength of the nanocomposites by preventing grain boundary shear ("sliding"). The hardness enhancement in the heterostructures is usually explained by the Koehler's model [9].

The 1 ML thick SiN_x tissue in the TiN/SiN_x nanocomposites with randomly oriented TiN nanocrystals appears amorphous in X-ray and electron diffraction (XRD and ED) [1, 10], whereas it is heteroepitaxially stabilized in the heterostructures [4]. The maximum hardness is achieved when the SiN_x layer is about 1 ML thick, but the hardness enhancement is lost when the thickness reaches 2 ML (see [1] and references therein) due to the weakening of neighbor Ti-N bonds (see Ref. [8]. The possibility of the formation of the epitaxial interfaces in TiN/SiN heterostructures has been discussed in Ref. [4,11-14]. Both the coherent and incoherent TiN/SiN_x interfaces were widely investigated in the framework of different first-principles procedures which were summarized in Ref. [15].

Whereas the Ti-Al-Si-N and Cr-Al-Si-N nanocomposites find already large-scale industrial applications as wear-protection coatings on tools [16], the nanocomposite coatings based on Ti-Zr-N alloys were studied to a lesser extent. Sobol', Pogrebnjak and Bersenev showed that the Ti-Zr-N in Ti-Zr-N/SiN_y nanocomposite coatings form B1-$Ti_xZr_{1-x}N$ solid solution [17] with maximum nanohardness of about 40 GPa.

Because the investigation of the ternary nanocomposite M1-M2-N/SiN_x, (M1, M2 are transition metals) is in its infancy, we investigate in the present paper the $Ti_xZr_{1-x}N/SiN_y$ heterostructures as a model systems using first-principles quantum molecular dynamics (QMD) calculations.

2. COMPUTATATIONAL ASPECTS

First-principles QMD calculations of the electronic structure have been done using the Quantum-ESPRESSO code [18] for 8-atom cubic supercells of B1-$Ti_{4-n}Zr_nN_4$, n = 0, 1, 2, 3 and 4 random solid solution $Ti_{1-x}Zr_xN$, and for 105-atomic hexagonal-like supercells of B1-$Ti_nZr_{45-n}N_{45}(111)/Si_6N_9$, n = 0, 18, 27, and 45, representing the B1-$Ti_xZr_{1-x}N(111)$/ Si_3N_4-like Si_2N_3 heterostructures. The heterostructures with 1 monolayer of Si_3N_4-like Si_2N_3 interfacial layer between five monolayers thick B1-$Ti_xZr_{1-x}N(111)$, x = 1.0, 0.6, 0.4 and 0.0, slabs were investigated using first-principles QMD with the structure optimization as described in [18]. Several heterostructures with the partially segregated ("ordered") and random arrangement of the atoms within B1-$Ti_xZr_{1-x}N(111)$ slabs were considered. The "ordered" structures were composed of the TiN and ZrN slabs. The atomic configurations of the heterostructures under consideration are shown in Figs. 1 to 3. Vanderbilt ultra-soft pseudo-potentials were used to describe the electron-ion interaction [19]. In the Vanderbilt approach [14], the orbitals are allowed to be as soft as possible in the core regions so that their plane-wave expansion converges rapidly. The semi-core states were treated as valence states. For the titanium and zirconium pseudo-potentials, the nonlinear core-corrections were taken into account [18]. To describe exchange-correlation energy, the generalized gradient approximation (GGA) of Perdew et al. [20] has been employed. The criterion of conver-

gence for the total energy was 10^{-6} Ry/formula unit. To speed up the convergence, each eigenvalue was convoluted with a Gaussian with a width of 0.02 Ry. The cut-off energy for the plane-wave basis was set to 60 Ry and 30 Ry, for the 8- and 105-atomic unit supercells, respectively. The integration in the Brillouin zone (BZ) was done on special **k**-points determined according to the Monkhorst-Pack scheme [21] using a mesh (8 8 8) for the 8-atomic supercells, and (2 2 2) for the 105-atomic supercells.

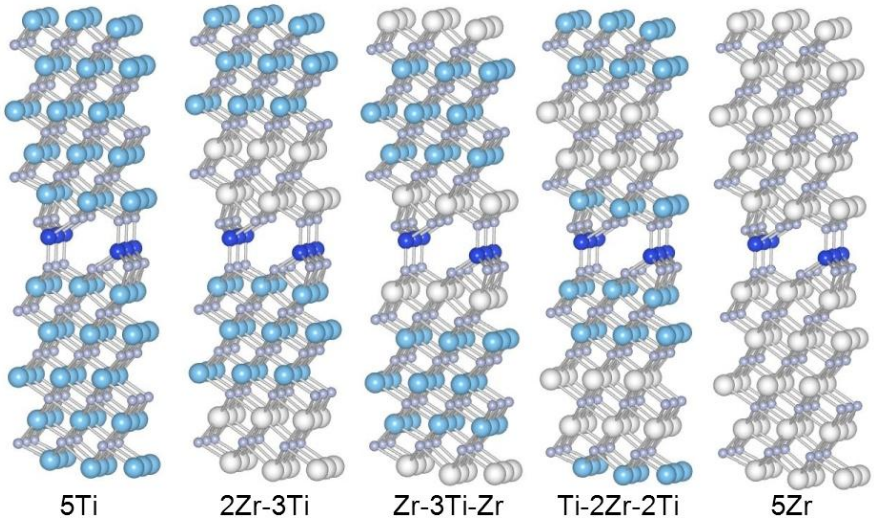

Fig. 1 – (Color online) Atomic configurations of heterostructures consisting of TiN slabs ("5Ti" on the left), the partially segregated ("ordered") Ti-rich ($Ti_{27}Zr_{18}N_{45}/Si_6N_9$) slabs, and ZrN slabs ("5Zr" on the right). The denotation of the heterostructures gives the sequence of layers in the c-direction. Here and in further figures are: N-the small circles, Si-dark circles, Ti-dark large circles, Zr-light large circles

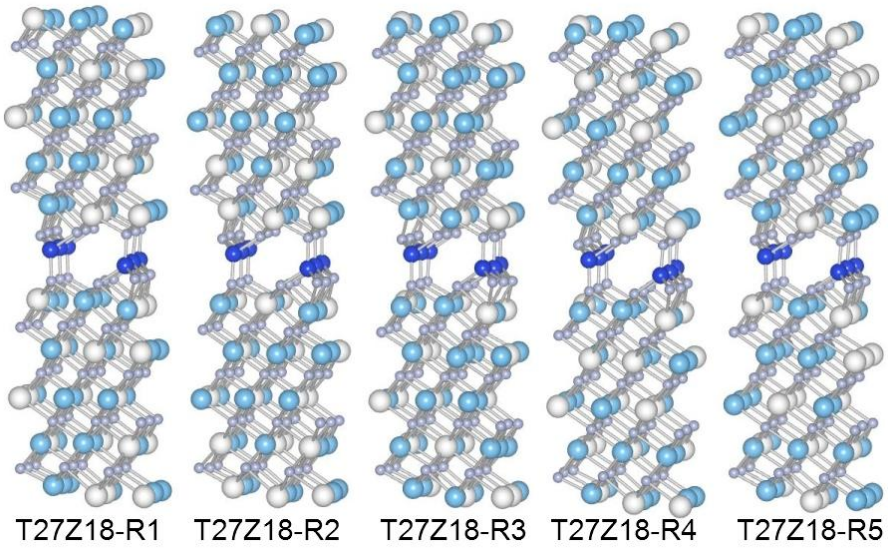

Fig. 2 – (Color online) Atomic configurations of the Ti-rich random $Ti_{27}Zr_{18}N_{45}/Si_6N_9$ solution based heterostructures. The Zr-rich heterostructures are constructed from the corresponding Ti-rich heterostructures. In the denotation of the heterostructure, T and Z are Ti and Zr, respectively, and the numbers are their concentrations

The QMD calculations of the initial relaxed heterostructures are carried out at 1400 K with fixed unit cell parameters and volume (NVT ensemble, i.e., constant number of particles-volume-temperature) for ~ 2.5 ps. In all the QMD calculations, the time step was about 10^{-15} s. The system temperature is kept constant by rescaling the velocity. For the large-scale system calculations, only the Γ point is taken into account in the BZ integration. The variation of the total energy has been considered during each QMD time step. During the initial 1 to 1.5 ps, all structures reached closely their equilibrium state and, at later times, the total energy of the equilibrated structures varied only slightly around the constant equilibrium value with small amplitude of 0.025 eV/atom.

After QMD equilibration, the geometry of all the

hetero-structures has been optimized by simultaneously relaxing the atomic basis vectors and the atomic positions inside the unit cells using the BFGS algorithm [22]. The relaxation of the atomic coordinates and of the unit cell is considered to be complete when the atomic forces are less than 1.0 mRy/Bohr (25.7 meV/Å), the stresses are smaller than 0.05 GPa, and the total energy during the iterative structural optimization process is changing by less than 0.1 mRy (1.36 meV).

The formation energy of the $Ti_{1-x}Zr_xN$ solid solution (E_{Form}) and of the heterostructures (E_{hetero}) was determined from Eqs. (1a) and (1b), respectively,

$$E_{Form}(x) = E_T(Ti_{1-x}Zr_xN) - (1-x)E_T(TiN) - xE_T(ZrN)\,, \tag{1a}$$

$$E_{hetero}(x) = E_T(Ti_{1-x}Zr_xN / SiN_y) - (1-x)E_T(TiN / SiN_y) - xE_T(ZrN / SiN_y)\,, \tag{1b}$$

as a function of composition x. Here, E_T is the total energy of the $Ti_{1-x}Zr_xN$ solid solutions, of the stoichiometric TiN and ZrN compounds, and of the $Ti_{1-x}Zr_xN/SiN_y$, TiN/SiN_y and ZrN/SiN_y heterostructures.

3. RESULTS AND DISCUSSION

In Fig. 3, we show the concentration dependence of the lattice parameter a for $Ti_{1-x}Zr_xN$ solid solution. The calculated values are slightly higher than the experimental ones by approximately 0.2-0.5 %, and display a slight positive deviation from the mixing rule $a(x)=x\cdot a_{ZrC} + (1-x)\cdot a_{TiC}$, in agreement with the experiment [5].

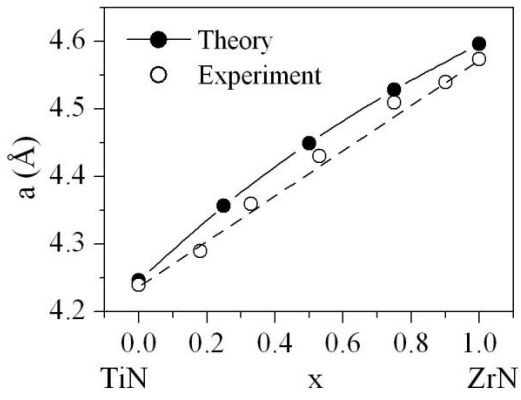

Fig. 3 – Lattice parameters of $Ti_{1-x}Zr_xN$ versus composition. The experimental data were taken from Ref. [5]. The dashed line reflects the mixing rule for the experimental results. Here and in the following figures the solid line is a polynomial fit to the data points

The Gibbs free energy of mixing of $Ti_{1-x}Zr_xN$, calculated at zero temperature (i.e. formation energy), as a function of composition x is shown in Fig. 4. The formation energy is positive in the entire composition range, which implies that the alloys are metastable, and should decompose into TiN and ZrN with the chemical driving force E_{Form}, in agreement with the theoretical results in Ref. [5]. Because the mixing entropy term stabilizes the solid solution, and this stabilization increases with increasing temperature, the positive value of the Gibbs free energy in Fig. 4 is due to the mixing enthalpy term.

We performed the QMD optimization of the structure of the initial epitaxial heterostructures at zero temperature and at 1400 K with subsequent variable-cell structural relaxation. The arrangement for all interfaces was found to be preserved, as shown in Figs. 1 and 2. The structural parameters and the total energies of the computed heterostructures are summarized in Tables 1 to 3. One can see from Tables 2 and 3 that, for the same concentration x, the structural parameters weakly depend on the atomic arrangements. The average cell volume for the disordered structures is higher as compared to that of the ordered one.

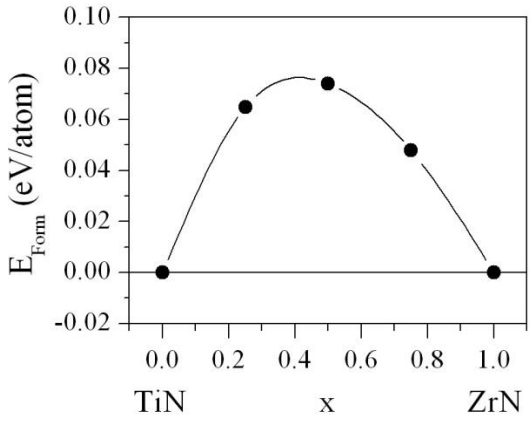

Fig. 4 – Computed formation energy (E_{Form}) for $Ti_{1-x}Zr_xN$ as a function of composition *x*

The total energy calculations show that the Ti-Zr-N solid solution, which forms during the deposition, is metastable and should decompose into stoichimetric TiN and ZrN. However, by analogy with other similar systems, such as Ti-Al-N and Cr-AlN, this decomposition is activated and therefore it will occur only at somewhat higher temperature. (Of course, the mixing entropy term will stabilize the random solid solution at high temperatures approaching the melting point, where the de-stabilizing mixing entropy term will diminish.) However, in the $Ti_{1-x}Zr_xN/SiN_x$ heterostructures, the different stability of heterostructures consisting of ordered and random $Ti_{1-x}Zr_xN$ solid solution slabs terminated with either Zr or Ti atoms at the SiN_x interface indicate that the decomposition of the random solid solution may be promoted already at a lower temperature.

Finally, we would like to emphasize that our estimate of the stability of the $Ti_{1-x}Zr_xN$ solid solution is based on the comparison of the total energies of different heterostructures. For a more detailed analysis the vibrational and configuration entropies should be taken into account.

Table 1 – Structural parameters and total energy of the $Ti_{45}N_{45}/Si_6N_9$ (5Ti) and $Zr_{45}N_{45}/Si_6N_9$ (5Zr) heterostructures (see Fig. 1)

	A (Å)	B (Å)	C (Å)	V (Å^3/at)	E_T (eV/at)
5Ti	8.974	8.915	14.863	9.826	-828.32506
5Zr	9.730	9.607	15.865	12.263	-726.32889

Table 2 – Structural parameters and total energy of the $Ti_{27}Zr_{18}N_{45}/Si_6N_9$ (i.e. $Ti_{0.6}Zr_{0.4}N/Si_2N_3$) heterostructures (see Figs. 1 and 2)

($0.6 \times E_T(Ti_{45}N_{45}/Si_6N_9) + 0.4 \times E_T(Zr_{45}N_{45}/Si_6N_9) = -787.52659$ eV/at.)

Heterostructure	a(Å)	b(Å)	c(Å)	V(Å^3/at)	E_T(eV/at)
2Zr-3Ti	9.292	9.202	15.291	10.813	-787.48378
Zr-3Ti-Zr	9.278	9.192	15.337	10.814	-787.48502
Ti-2Zr-2Ti	9.319	9.217	15.238	10.824	-787.48505
Average	9.297	9.203	15.289	10.817	-787.48462
T27Z18-R1	9.311	9.215	15.316	10.873	787.48835
T27Z18-R2	9.315	9.214	15.300	10.856	-787.48945
T27Z18-R3	9.313	9.218	15.325	10.885	-787.48422
T27Z18-R4	9.318	9.202	15.355	10.904	-787.47507
T27Z18-R5	9.314	9.212	15.345	10.887	-787.47476
Average	9.314	9.212	15.328	10.881	-787.48237

Table 3 – Structural parameters and total energy of the $Ti_{18}Zr_{27}N_{45}/Si_6N_9$ (i.e. $Ti_{0.4}Zr_{0.6}N/Si_2N_3$) heterostructures (see Figs. 1 and 2)

($0.4 \times E_T(TiN/Si_2N_3) + 0.6 \times E_T(ZrN/Si_2N_3) = -767.12736$ eV/at).

Heterostructure	a (Å)	b (Å)	c (Å)	V (Å^3/at)	E_T (eV/at)
2Ti-3Zr	9.451	9.345	15.491	11.316	-767.08720
Ti-3Zr-Ti	9.463	9.355	15.439	11.306	-767.08859
Zr-2Ti-2Zr	9.425	9.324	15.568	11.309	-767.08491
Average	9.446	9.341	15.499	11.310	-767.08690
T18Z27-R1	9.464	9.356	15.505	11.365	-767.08819
T18Z27-R2	9.472	9.343	15.520	11.355	-767.08647
T18Z27-R3	9.463	9.352	15.512	11.359	-767.09296
T18Z27-R4	9.466	9.367	15.487	11.363	-767.09835
T18Z27-R5	9.465	9.363	15.497	11.353	-767.09782
Average	9.466	9.356	15.504	11.359	-767.09276

CONCLUSIONS

We performed first-principles investigations of the B1-$Ti_xZr_{1-x}N(111)/Si_3N_4$-like Si_2N_3 heterostructures for x = 1.0, 0.6, 0.4 and 0.0, and of the B1-$Ti_xZr_{1-x}N$ solid solutions for x = 1.0, 0.75, 0.5, 0.25 and 0.0. Several heterostructures with the segregated ("ordered") and random arrangement of the atoms within B1-$Ti_xZr_{1-x}N(111)$ slabs were considered. The ordered structures consisted of TiN and ZrN layers. The ordered heterostructures, in which the Zr atoms surround the SiN_x interface, were found to be most stable. According to our results, the B1-$Ti_xZr_{1-x}N(111)/Si_3N_4$-like Si_2N_3 nanostructures should decompose into the $TiN(111)/SiN_y$ and $ZrN(111)/SiN_y$ units due to the immiscibility of TiN and ZrN. However, experiment shows that during the deposition at relatively low temperature the B1-$Ti_xZr_{1-x}N$ metastable solid solutions can form. According to our results, the formation of the random B1-$Ti_xZr_{1-x}N$ solid solution will be preferable for the Zr-rich heterostructures, whereas for the Ti-rich heterostructure the ordered alloys should form.

ACKNOWLEDGEMENTS

This work was supported by the STCU Contract, No. 5539. We thank Dr. Maritza G. J. Veprek-Heijman for valuable comments to the manuscript.

REFERENCES

1. S. Veprek, M.G.J. Veprek-Heijman, P. Karvankova, J. Prochazka, *Thin Solid Films* **476**, 1 (2005).
2. S. Veprek, R.F. Zhang, M.G.J. Veprek-Heijman, S.H. Sheng, A.S. Argon, *Surf. Coat. Technol.* **204**, 1898 (2010).
3. Y.-H. Chen, K.W. Lee, W.-A. Chiou, Y.-W. Chung, L.M. Keer, *Surf. Coat. Technol.* **146-147**, 209 (2001).
4. H. Söderberg, M. Odén, J.M. Molina-Aldareguia, L. Hultman, *J. Appl. Phys.* **97,** 114327 (2005).
5. A. Hoerling, J. Sjölén, H. Willman, T. Larson, M. Odén, L. Hultman, *Thin Solid Films* **516**, 6421 (2008).
6. T. An, M. Wen, L.L. Wang, C.Q. Hu, H.W. Tian, W.T. Zheng, *J. Alloys Compounds* **486**, 515 (2009).
7. S. Veprek, A.S. Argon, R.F. Zhang, *Philos. Mag. Lett.* **87**, 955 (2007).
8. R.F. Zhang, A.S. Argon, S. Veprek, *Phys. Rev. Lett.* **102**, 015503 (2009); *Phys. Rev. B* **79**, 245426 (2009); c: ibid, **81**, 245418 (2010).
9. J.S. Koehler, *Phys. Rev. B* **2**, 547 **(**1970).
10. S. Veprek, S. Reiprich, *Thin Solid Films* **268**, 64(1995).
11. L. Hultman, J. Barenõ, A. Flink, H. Söderberg, K. Larsson, V. Petrova, M. Odén, J.E. Greene, I. Petrov, *Phys. Rev. B*

75, 155437 (2007).
12. H. Söderberg, M. Odén, T. Larsson, L. Hultman, J.M. Molina-Aldareguia, *Appl. Phys. Lett.* **88**, 191902 (2006).
13. H. Söderberg, M. Odén, A. Flink, J. Brich, P.O.A. Persson, M. Beckers, L. Hultman, *J. Mater. Res.* **22**, 3255 (2007).
14. X. Hu, H. Zhang, J. Dai, G. Li, M. Gu, J. Vac. *Sci. Technol. A* **23**, 114 (2005).
15. V.I. Ivashchenko, S. Veprek, P.E.A. Turchi, V.I. Shevchenko, *Phys. Rev. B* **85**, 195403 (2012).
16. S. Veprek, M.G.J. Veprek-Heijman, *Surf. Coat. Technol.* **202**, 5063 (2008).
17. O. V. Sobol', A. D. Pogrebnyak and V. M. Beresnev, *The Physics of Metals and Metallography* **112**, 188 (2011).
18. S. Baroni, A. Dal Corso, S. de Gironcoli, P. Giannozzi, C. Cavazzoni, G. Ballabio, S. Scandolo, G. Chiarotti, P. Focher, A. Pasquarello, K. Laasonen, A. Trave, R. Car, N. Marzari and A. Kokalj, http://www.pwscf.org/.
19. D. Vanderbilt, *Phys. Rev. B* **41**, 7892 (1990).
20. J.P. Perdew, K. Burke, M. Ernzerhof, *Phys. Rev. Lett.* **77**, 3865(1996).
21. H.J. Monkhorst, and J.D. Pack, *Phys. Rev. B* **13**, 5188 (1976).
22. S.R. Billeter, A. Curioni, W. Andreoni, *Comput. Mater. Sci.* **27**, 437 (2003).